Carcinogenic dioxane detection using pristine and metal-doped 2D VSe2: Insights from density functional theory simulations

Sreejith Pallikkara Chandrasekharan, Seetha Lakshmy, Saju Joseph, Nandakumar Kalarikkal

AIP Advances

RESEARCH ARTICLE | JUNE 16 2023

Carcinogenic dioxane detection using pristine and metal-doped 2D VSe_2: Insights from density functional theory simulations

Special Collection: 2022 Chemical Physics

Sreejith Pallikkara Chandrasekharan ; Seetha Lakshmy ; Saju Joseph ; Nandakumar Kalarikkal

AIP Advances 13, 065024 (2023)
https://doi.org/10.1063/5.0139779

Carcinogenic dioxane detection using pristine and metal-doped 2D VSe_2: Insights from density functional theory simulations

Cite as: AIP Advances 13, 065024 (2023); doi: 10.1063/5.0139779
Submitted: 24 December 2022 • Accepted: 1 June 2023 •
Published Online: 16 June 2023

Sreejith Pallikkara Chandrasekharan[1,2] Seetha Lakshmy,[1] Saju Joseph[1,3a)] and Nandakumar Kalarikkal[1,3,4a)]

AFFILIATIONS

[1] International and Inter University Centre for Nanoscience and Nanotechnology, Mahatma Gandhi University, Kottayam, Kerala 686 560, India
[2] Univ. Rennes, INSA Rennes, CNRS, Institut FOTON – UMR 6082, F-35000 Rennes, France
[3] School of Nanoscience and Nanotechnology, Mahatma Gandhi University, Kottayam, Kerala 686 560, India
[4] School of Pure and Applied Physics, Mahatma Gandhi University, Kottayam, Kerala 686 560, India

[a)] **Authors to whom correspondence should be addressed:** nkkalarikkal@mgu.ac.in and psajujoseph@gmail.com

ABSTRACT

Dioxane (diethylene oxide) is a synthetic organic compound classified as heterocyclic ether, a potentially carcinogenic water toxicant. Prolonged exposure can cause eye irritation, carcinogenic liver reactions, and other severe issues. Therefore, efficient dioxane detectors are needed to be designed and developed. Inspired by the recent developments of 2D materials in biosensing, in this work, the dioxane detection potentiality of pristine and metal-doped (Al, Au, and Ag) 2D VSe_2 have been systematically examined using Density Functional Theory (DFT) based simulations. Among all the metallic dopants considered, Al binds energetically on the VSe_2 surface with an energy of −2.158 eV. The adsorption of dioxane was studied by considering the electronic properties, adsorption energy, orbital interactions, and charge transfer. Our DFT calculation suggests that dioxane adsorption in Al-doped VSe_2 is more promising than the pristine and other metal-doped VSe2 systems, due to the reasonable adsorption energy of −0.80 eV, charge transfer of −0.567*e*, and strong orbital interaction between Al 3*p* and O 2*p* orbitals. Additionally, the room temperature structural solidity of the sensor has also been verified using the *ab initio* molecular dynamics simulations. The reported theoretical results inspire the fabrication and engineering of efficient dioxane sensors using Al-doped VSe_2.

I. INTRODUCTION

Rapid industrialization and population growth resulted in the discharge of large quantities of organic pollutants, undeniably contributing to water resource pollution.[1–3] Diethylene oxide (widely known as dioxane or 1,4-dioxane), classified as ether, with the chemical formula $C_4H_8O_2$, is a colorless liquid with a soft sweet smell like dimethyl ether. Dioxane is used on a large scale to produce paper, textiles, electronics, cosmetics, etc. They are often regarded as a powerful solvent and stabilizer for chlorinated solvents in laboratory applications. It is well known that dioxane is an environmental water toxicant with high water solubility, hydrophilicity, long-term stability, and non-bio-degradability. Their excess presence can contaminate the ground, surface, and drinking water and are highly dangerous to living beings. Long term exposure can elicit severe eye irritation and carcinogenic reactions in the liver in various species. As per the studies, nearly one-fifth of the public drinking water sources in the United States (US) have measurable quantities of dioxane.[4] The International Agency for Research on Cancer (IARC) and the US Environmental Protection Agency (USEPA) have categorized dioxane as a potential human carcinogen.[5] Moreover, the Agency for Toxic Substances and Disease Registry (ATSDR) designated dioxane as a superfund precedence category due to the chemical harmful effects and proclivity to pollute drinking water.[4] Because

of these implications, it is urgent to develop sensors that selectively detect and remove the dioxane molecules from the environment.

In recent years, many sophisticated physicochemical and biological approaches have been used to successfully remove dioxane from affected environments. The unique chemical features of dioxane, such as its low Henry's law constant, high water solubility, and coexistence with the chlorinated solvents and other contaminants, make efficient removal difficult.[6] Complex water treatment procedures can be utilized to eradicate trace contaminants of dioxane.[5] Some of these include the photoinduced oxidation method (UV/H_2O_2) to substantially eliminate the structure of organic chemical; and, the Fenton's reagent (Fe and H_2O_2), advanced oxidation processes using systems, such as ozone (O_3)/H_2O_2), and H_2O_2 – TiO_2 combined vacuum UV. The sonolytic decomposition chemistry of dioxane in an aqueous solution has also been investigated,[7] where dioxane is dissolved into smaller short-chain organic by-products using ultrasound, which can subsequently be destroyed more successfully by other methods like biological processes. Although several other advanced dioxane removal technologies, such as solid-phase microextraction (SPME), distillation, gas chromatography (GC), thermal methods, air stripping and membrane filtration techniques, etc., are incompetent due to their high rate of cost and energy consumption.[8–11] Recent studies including electrochemical dioxane-detection by using nickel oxide doped on neodymium oxide nanocomposites ($NiO@Nd_2O_3$ NCs) embedded on glassy carbon electrode[12] and reduced graphene oxide–curcumin nanocomposite synthesized by a simple solution approach[13] promotes the need of developing this water pollutant.

However, properties, such as binding energy, adsorption geometry, adsorption configuration, charge transfer, etc., for detecting biomolecules cannot be directly determined by the time-consuming real experiment methods. Computational techniques are the best way to perform quantum mechanical calculations to analyze materials' various properties and phenomena and model them.

In this study, we have adopted the widely applicable quantum mechanical theoretical simulation approach called Density Functional Theory (DFT)[14] to analyze the molecular interactions. In these first-principle based calculations, the energy is represented as functionals of density. Many theoretical investigations have recently been conducted to search for novel materials for sensing applications. Interestingly, some cutting-edge theoretical research on SiCNT was conducted utilizing DFT simulations to examine the adsorption and removal of dioxane.[15] Furthermore, the DFT-D3/revPBE calculation is verified using the MP2 theoretical method. The study showed that dioxane has significant adsorption toward this nanotube, but the higher recovery time limits the practical usage. However, most traditional sensing materials have several flaws due to their low sensitivity and selectivity. The interaction of biomolecules with 2D material is mainly via physisorption because of weak van der Waals forces. By modifying the functional qualities of 2D materials, such as defects engineering hybrid structure formation, the adsorption performances of these materials may be enhanced. Usually, metallic doping methods are adopted in the studies of 2D materials. Its unique and robust coupling of electromagnetic properties gives a charge transferring nature. They form covalent bonds with neighboring atoms via charge transfer, improving the conductivity of the pristine 2D material and hence the sensing properties.

Transition-metal dichalcogenides (TMDCs) are emerging 2D materials with a stoichiometric formula of MX_2. M denotes a transition metal element, such as Sc, V, Mo, Ti, or W, while X stands for a chalcogen element, such as Te, Se, or S. Here, a single layer of M atoms is stacked between the bi-layer of X atoms in this tri-layered structure, creating the layered structure X-M-X. Long-range van der Waals (VdW) forces dominate between these layers, resulting in the weak interaction. It exhibits unique photoelectronic, thermal, chemical, and mechanical properties,[16,17] making it promising for gas or biosensing applications.[18–20] The uniqueness of TMDCs is due to the presence of the *d* orbitals of the heavy metals, which causes a robust spin–orbit interaction, leads to valley polarization. The TMDCs have out-of-plane and broken in-plane mirror symmetry. The polymorphic nature of TMDC structures is a fascinating feature. TMDCs can be mainly classified into two structural phases: 2H and 1T.[21,22] The 2H is semiconducting, and the coordination of metal atoms is trigonal prismatic, while the 1T structure is metallic with octahedral coordination. In view of the above, it is reasonable to conclude that TMDCs offer enormous untapped potential as a future choice for numerous biomolecule sensing applications with their wide range of characteristics.

2D vanadium dichalcogenides (VX_2), such as VSe_2, VTe_2, and VS_2, have recently attracted much interest[23–26] due to their exceptional optical, electrical, and chemical characteristics. Our research focused on the 1T VSe_2 monolayer, a paramagnetic material where the vanadium atoms are surrounded by a trigonally deformed cage of selenium atoms in an octahedral environment.[27] Zhang *et al.*[28] used a chemical vapor deposition (CVD) approach to establish a van der Waals epitaxial strategy for synthesizing stable 1T VSe_2 nanosheets on mica. Surprisingly, these 2D structures have exceptional metallic characteristics, including the electrical conductivity up to 10^6 S m^{-1}, higher than the other conductive 2D materials. Synthesizing VSe_2 monolayer also have been reported by effective methods, such as liquid exfoliation,[29] from $[(SnSe)_{1.15}]_m(VSe_2)_n]$ ferecrystals via physical vapor deposition,[30] low-pressure chemical vapor deposition (LPCVD),[31] etc. In very recent work, the potential of 1T VSe_2 for nitrobenzene detection was explored.[26] The DFT study reveals that the transition metal doped VSe_2 is more sensitive to nitrobenzene molecules.

Although some significant observational facts exist for dioxane sensing studies, evidence of investigating TMDCs as a sensing material, particularly monolayered VSe_2, as a potential dioxane sensing material is unknown to the authors' available knowledge. In this current work, the adsorption and electronic properties of VSe_2 as a biosensor for dioxane have been examined using first principle-based DFT calculations. To overcome the weak interaction of VSe_2 monolayer toward dioxane, VSe_2 has been modified by doping with various metals (Al, Ag, Au, W, and Ti). Total Density of States (TDOS) and Partial Density of States (PDOS) analyses have been done to study the orbital interactions of states near the Fermi level and the charge transfer analysis via Lowdin Charge Analysis (LCA). Finally, because of its high adsorption energy toward dioxane, we suggest the Al-doped VSe_2 structure is among the most potential dioxane sensing materials. Furthermore, the structural durability of VSe_2 + Al was examined using *ab initio* MD simulations at 300 K, which revealed that the combination is extremely stable.

II. COMPUTATIONAL DETAILS

This study calculated all the structural, electronic, interfacial, and sensing properties of 2D VSe_2 and metal doped structures using DFT with the Quantum Espresso package.[32] As an exchange-correlation energy functional approximation, Perdew–Burke–Ernzerhof (PBE) in the Generalized Gradient Approximation (GGA) function (PBE-GGA) were used.[33] As per the literature, GGA is appropriate for accurately predicting the electronic, magnetic, and optical properties of 2D TMDCs. To accommodate the long-range van der Waal's interactions, Grimme DFT-D2 were also introduced in the calculations. For the current work, we have modeled a 2 × 2 supercell of 2D 1T VSe_2 monolayer containing 12 atoms. To eliminate the interactions between the periodic images, a 20 Å vacuum spacing is introduced in the vertical direction of the VSe_2 monolayer, i.e., in the z-direction. The plane-wave-cutoff energy was set to 35 Ry. The geometrical structures were relaxed until each atom's total computed energy and force were less than 10^{-6} and 10^{-4} eV, respectively. The Brillion zone integration was achieved by 4 × 4 × 1 Monkhrost–Pack. For the most promising system, molecular dynamic simulations at 300 K were also done to remark on the sensor material's integrity at ambient temperatures.

III. RESULTS AND DISCUSSION

A. Electronic and structural properties of VSe_2 monolayer

In this study, we have considered the 1T phase of pristine VSe_2, in which a layer of metal Vanadium is placed between two selenium sheets. The optimized 2 × 2 supercell structure of VSe_2 is displayed in Fig. 1(a). The obtained lattice constants are a = b = 3.334 Å, correlating neatly with published primitive cell experimental value, a = b = 3.356 Å[34] and a = b = 3.36 Å,[35] and indeed corresponds to the previously determined DFT calculated value of a = b = 3.328 Å.[23] The optimized V–Se bond length is 2.487 Å with the computed interlayer distance of 1.84 Å, matching the earlier available interlayer result of 1.56 Å.[35] The TDOS of VSe_2 have been calculated using the GGA + U approach (U value ≈ 3.5 eV for V[36]) and are displayed in Fig. 2. The continuous and asymmetric spin states at

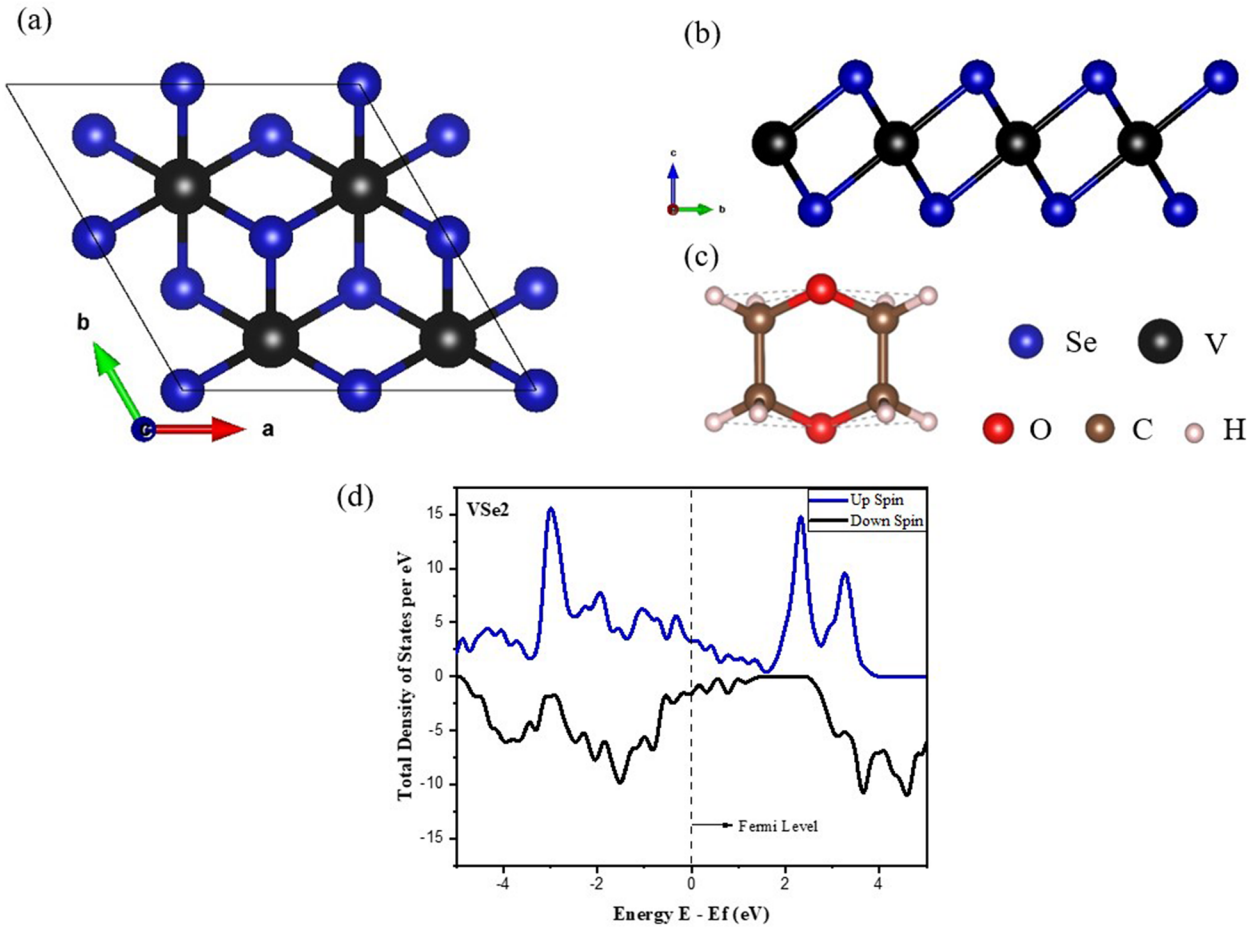

FIG. 1. The geometrically optimized structure of 1T VSe_2 monolayer in (a) armchair and (b) zigzag, (c) the relaxed structure of dioxane molecule, and (d) TDOS plot of 1T VSe_2.

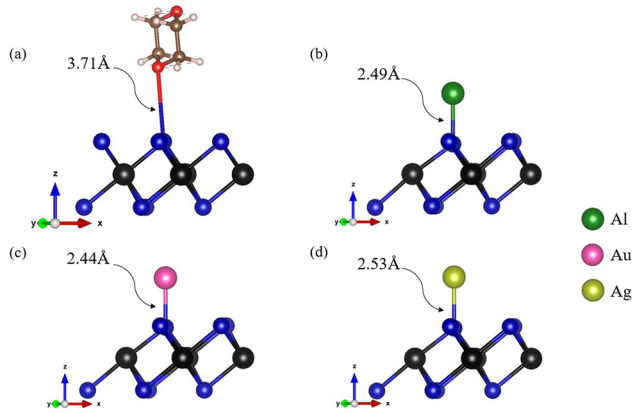

FIG. 2. Optimized structures of (a) dioxane adsorbed pristine VSe_2 and metal-doped VSe_2 after geometrical relaxation, (b) Al, (c) Au, and (d) Ag.

the Fermi level indicate that 1T VSe_2 is magnetic and metallic.[35] The reasonable match of pristine VSe_2 bond length and other electronic parameters with previously reported results gives us confidence in the simulation procedures and methods' accuracy. 1T MX_2 structure shows two major directions, armchair and zigzag. For the monolayer 1T VSe_2, the zigzag direction shows significantly stronger and more stretchy than armchair[37] [see Fig. 1(b)].

B. Adsorption studies of dioxane on pristine VSe_2

Here, we have placed the dioxane molecule ~2 Å above the surface of the pristine VSe_2 at four different adsorption sites: hcp, fcc, top, and hollow sites.[37] Several combinations of the initial structures were explored; for example, the O atom of the dioxane molecule is close to the different sites of VSe_2 and is geometrically relaxed to minimum energy configuration. The most stable geometric

TABLE I. DFT calculated adsorption energy and bond length of metal-doped VSe_2 systems.

System	Adsorption energy (eV)	Bond length (Å)
VSe_2 + Ti	+3.623	2.340 (Se–Ti)
VSe_2 + W	+7.388	2.285 (Se–W)
VSe_2 + Al	−2.158	2.495 (Se–Al)
VSe_2 + Au	−1.412	2.437 (Se–Au)
VSe_2 + Ag	−1.124	2.534 (Se–Ag)

structure of VSe_2 + dioxane/dopant is attained by the adsorption energy (E_{ad}) calculation using the following expression:

$$E_{ad}(D) = E(VSe_2 + D) - E(VSe_2) - E(D), \quad (1)$$

where $E(VSe_2)$, $E(D)$, and $E(VSe_2 + D)$ are, respectively, the energies of pristine VSe_2, dioxane molecule or dopant, and VSe_2 + dioxane/dopant system. Figure 2(a) depicts the DFT optimized structure of dioxane adsorbed VSe_2. The top site of Se with adsorption energy of −0.15 eV at a bond distance of 3.71 Å is found to be the most favorable position for the dioxane adsorption. The adsorption energy is negative, indicating that the adsorption is spontaneous and energetically feasible. The Density of States (DOS) of the VSe_2 gets altered after the dioxane adsorption, and it is clearly visible in Fig. 3(b). The adsorption configuration of dioxane molecules on the VSe_2 monolayer results in the transfer of charges between them. The LCA is performed to quantify the charge transfer between the dioxane and the pristine VSe_2 monolayer. As per the LCA, only a minute charge of 0.041*e* transfers from the VSe_2 to the dioxane molecule. The negligible charge transfer, weak adsorption energy, and large interaction distance suggest that the dioxane adsorption on pristine VSe_2 monolayer is physisorption, which would be due to the long-range van der Waal's forces. The practical implementation of the sensor requires

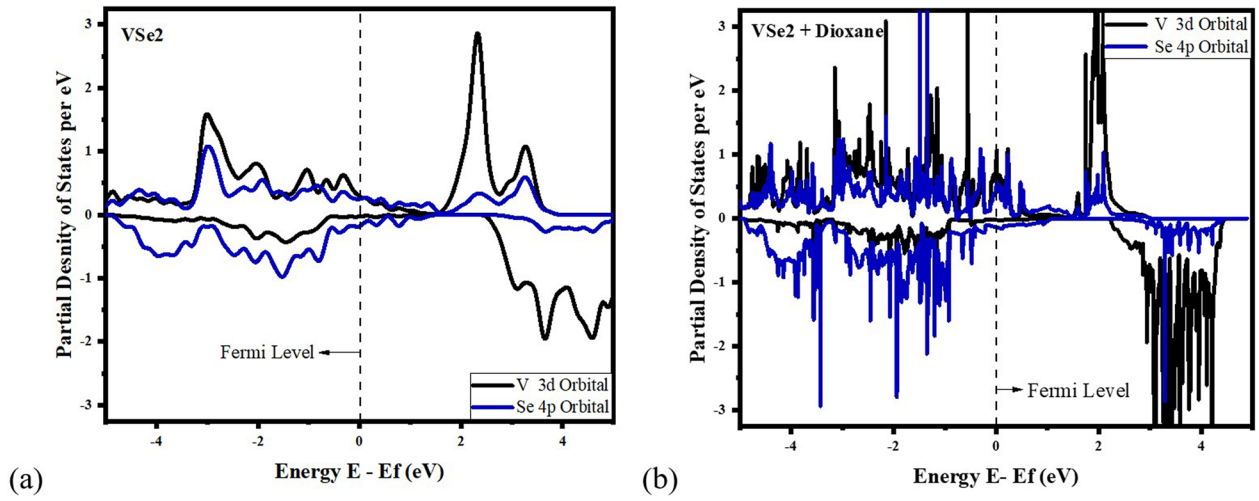

FIG. 3. PDOS plots of (a) pristine and (b) dioxane adsorbed VSe_2.

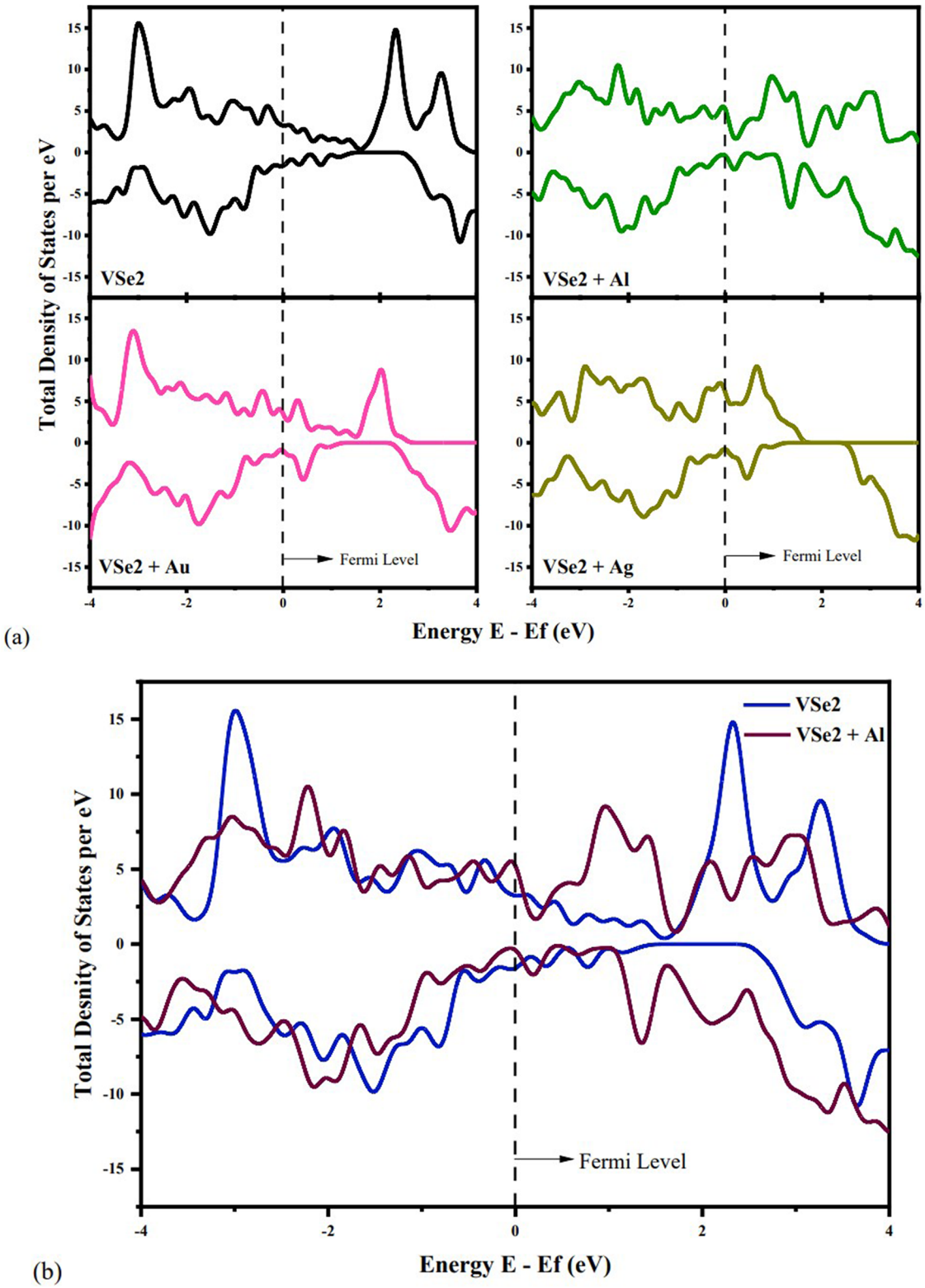

FIG. 4. TDOS plots for (a) pristine VSe_2, VSe_2 + Al, VSe_2 + Au, and VSe_2 + Ag systems (b) merged plots of pristine VSe_2 and VSe_2 + Al.

the dioxane molecules to be adsorbed strongly on the surface. In this respect, a metallic doping strategy was adopted.

C. Modification of the VSe_2 monolayer by metallic doping

We have placed metals, such as Al, Ag, Au, W, and Ti ~2 Å, above the VSe_2 surface at different adsorption sites and allowed the systems to relax. The adsorption energies and bond lengths for the best configuration of VSe_2 + metal are calculated using Eq. (1) and are shown in Table I. From adsorption calculations at different sites, it was found that the top site above the Se atom was the best site for doped metals Al, Au, and Ag. The W and Ti showed positive adsorption energies, implying that they do not bind on the VSe_2 surface. The corresponding relaxed structures of the metal-doped VSe_2 monolayer are illustrated in Figs. 2(b)–2(d). As per the calculated adsorption energy values, Al binds strongly on the VSe_2 monolayer with an energy of −2.158 eV. At the same time, the Au and Ag have comparatively low adsorption energy of −1.412 and −1.124 eV, respectively. Hence, the adsorption energy analysis confirms Al as the best dopant. Figure 4(a) denotes the TDOS of pristine and metal-doped VSe_2 systems. The improvement of energy states close to the Fermi level indicates the increase in conductivity of metal-doped VSe_2. The asymmetric spin states in the TDOS of VSe_2 + metal reminds the persistence of the magnetic nature. Additionally, Fig. 4(b) plots the TDOS plots of the pristine VSe_2 merged with the Al-doped VSe_2. Unlike the original VSe_2 monolayer, the DOS of the Al-doped system differs in several energy levels, with some significant increase in the Fermi level, which may be due to the electron exchange between the VSe_2 monolayer to the Al atom.

The PDOS analysis provides a clear idea of the orbital interactions and the direction of transfer of charges between the dioxane molecule and the substrate VSe_2. Figure 5 compares PDOS of the valance orbitals of VSe_2 (V 3*d* orbital and Se 4*p* orbital), 3*p* orbitals of isolated Al atom and Al atom in the VSe_2 + Al system. When the Al atom binds to the VSe_2 surface, a reduction in the energy states of the Al 3*p* orbital at the Fermi level occurs compared to that in the isolated Al atom. Simultaneously, the V 3*d* and Se 4*p* near the Fermi

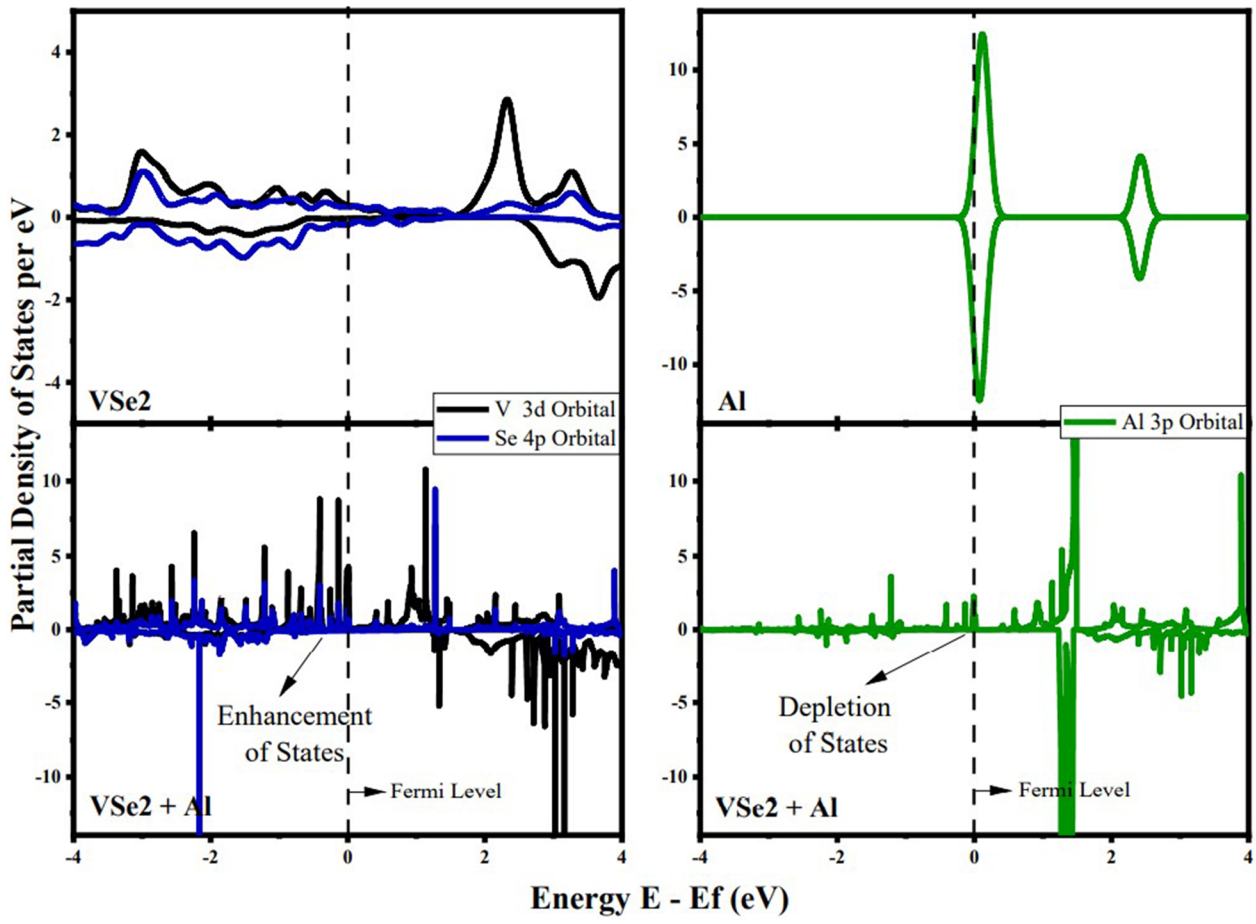

FIG. 5. The PDOS plots compare the valence orbitals of VSe_2 in the pristine and Al + VSe_2 system in the left panel, whereas in the right panel compare the 3*p* orbitals of isolated Al atom and the Al + VSe_2 system.

level get magnified, and the overall states are redistributed. This reduction in the Al and enhancement in VSe_2 energy states signifies a charge transfer from Al 3*p* orbital to 4*p* and 3*d* orbitals of Se and V in VSe_2 and is a result of the existence of an unpaired valence electron in the outermost *p* orbital. Hence, the Al atom tends to donate the electron and become an anion.

A similar redistribution of states can be observed from the PDOS plots of Au- and Ag-doped VSe_2 systems (supplementary material, Fig. S1). Since Au and Ag have an unpaired electron in their valence *s* orbitals, they can either act as an electron donator or an acceptor. On interacting with the VSe_2 system, the energy states of both the metals got depleted around the Fermi level (right panel of Fig. S1). This indicates the charge donating behavior of the Au and Ag metals. At the same time, the increased energy states near the Fermi level of the valence orbitals of the V and Se in VSe_2 denote the charge accumulation (left panel of Fig. S1), i.e., the VSe_2 gains charge from Au and Ag's 6*s* and 5*s* orbitals, respectively. According to the LCA, the Al atom loses a charge of 0.299*e* to the VSe_2 system.

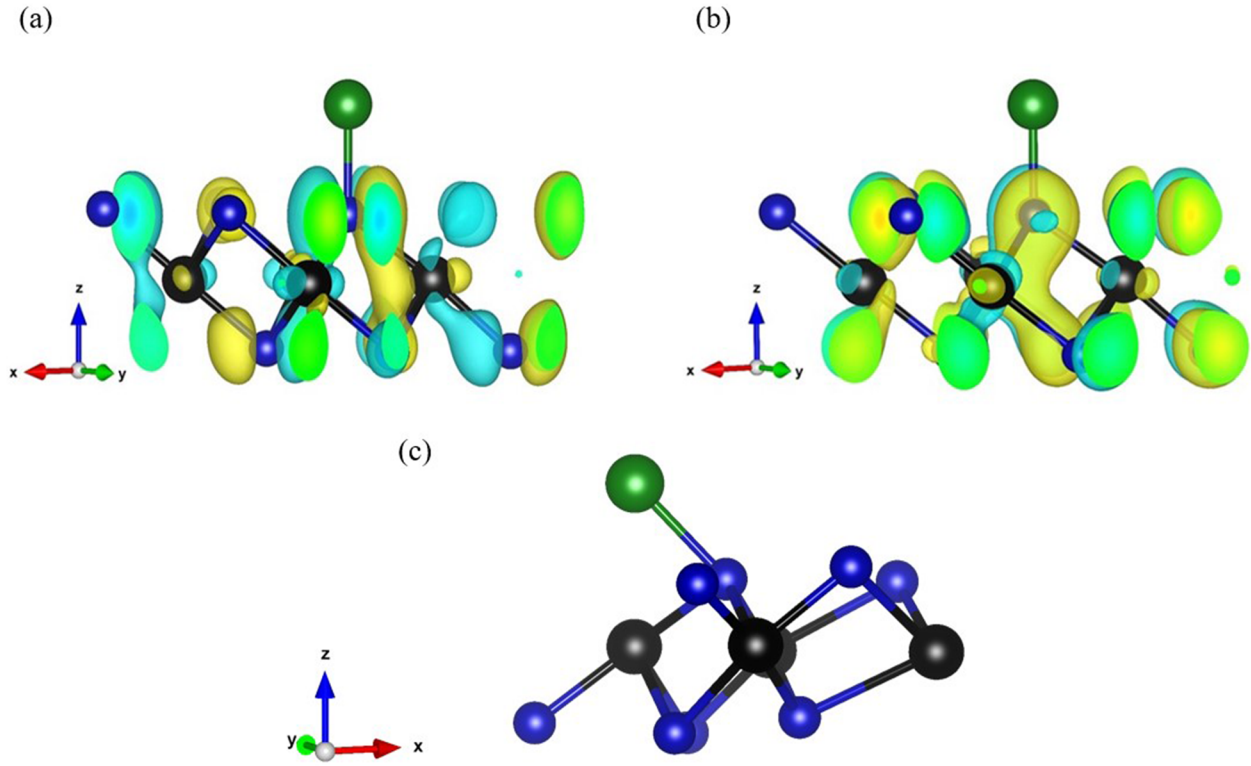

FIG. 6. The HOMO (a), LUMO (b), figures and MD snapshot at 300 K (c) of Al-doped VSe_2.

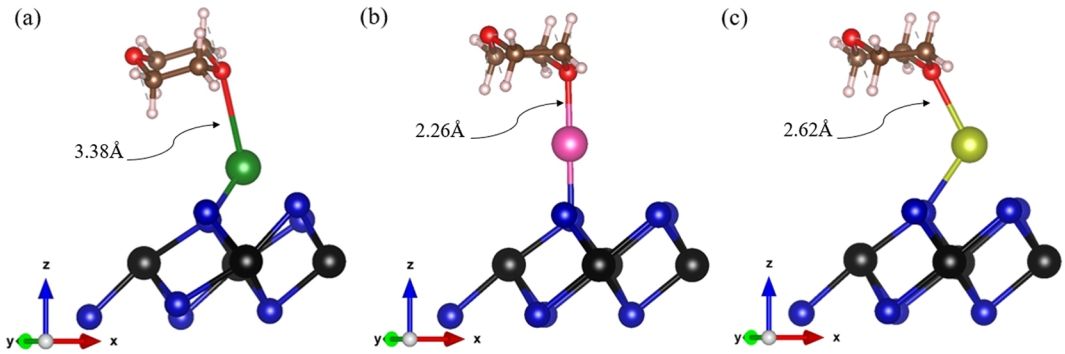

FIG. 7. Optimized structures of dioxane adsorbed (a) VSe_2 + Al, (b) VSe_2 + Au, and (c) VSe_2 + Ag systems.

In contrast, Au and Ag lose about 0.173*e* and 0.145*e*, respectively, to VSe_2 systems. The results obtained from LCA are pretty consistent with the PDOS.

Figures 6(a) and 6(b), respectively, shows the HOMO (highest occupied molecular orbital) and LUMO (lowest unoccupied molecular orbital) distributions of the Al-doped VSe_2 system. It is noted that a significant portion of HOMO and LUMO, basically the electron receiving/donating part, is distributed near the Se atom to which the Al is bonded. This signifies that the addition of Al atom enriched the active region on the VSe_2 surface and hence the sensitivity of the material. All the DFT calculations were performed at 0 K; therefore, it is highly essential to see the structural stability at ambient temperatures. Desorption of the molecules from the sensor materials is usually achieved by heating the material to higher temperatures. This also requires the consistency of the system at a higher temperature. To establish the same, we performed the *ab initio* Molecular Dynamics (AIMD) simulations at 300 K for the best system, i.e., VSe_2 + Al system. Figure 6(c) depicts the MD snapshot of the VSe_2 + Al system for 3 ps. Although the structural plot of VSe_2 + Al shows minor bond length variations due to the thermal agitations, the system remains stable without any distortion at 300 K. Therefore, the Al-doped VSe_2 system is quite feasible for practical sensor applications.

TABLE II. The adsorption energy and bond length of dioxane adsorbed pristine and metal-doped VSe_2 systems.

System	Adsorption energy (eV)	Bond length (Å)
Pristine VSe_2 + dioxane	−0.15	3.71 (Se–O)
VSe_2 +Al + dioxane	−0.80	3.38 (Al–O)
VSe_2 +Au + dioxane	−0.30	2.26 (Au–O)
VSe_2 +Ag + dioxane	−0.20	2.62 (Ag–O)

D. Adsorption of dioxane on metal-doped VSe_2

To observe the dioxane adsorption on the metal-doped VSe_2 system, we have placed the dioxane molecule above the structurally

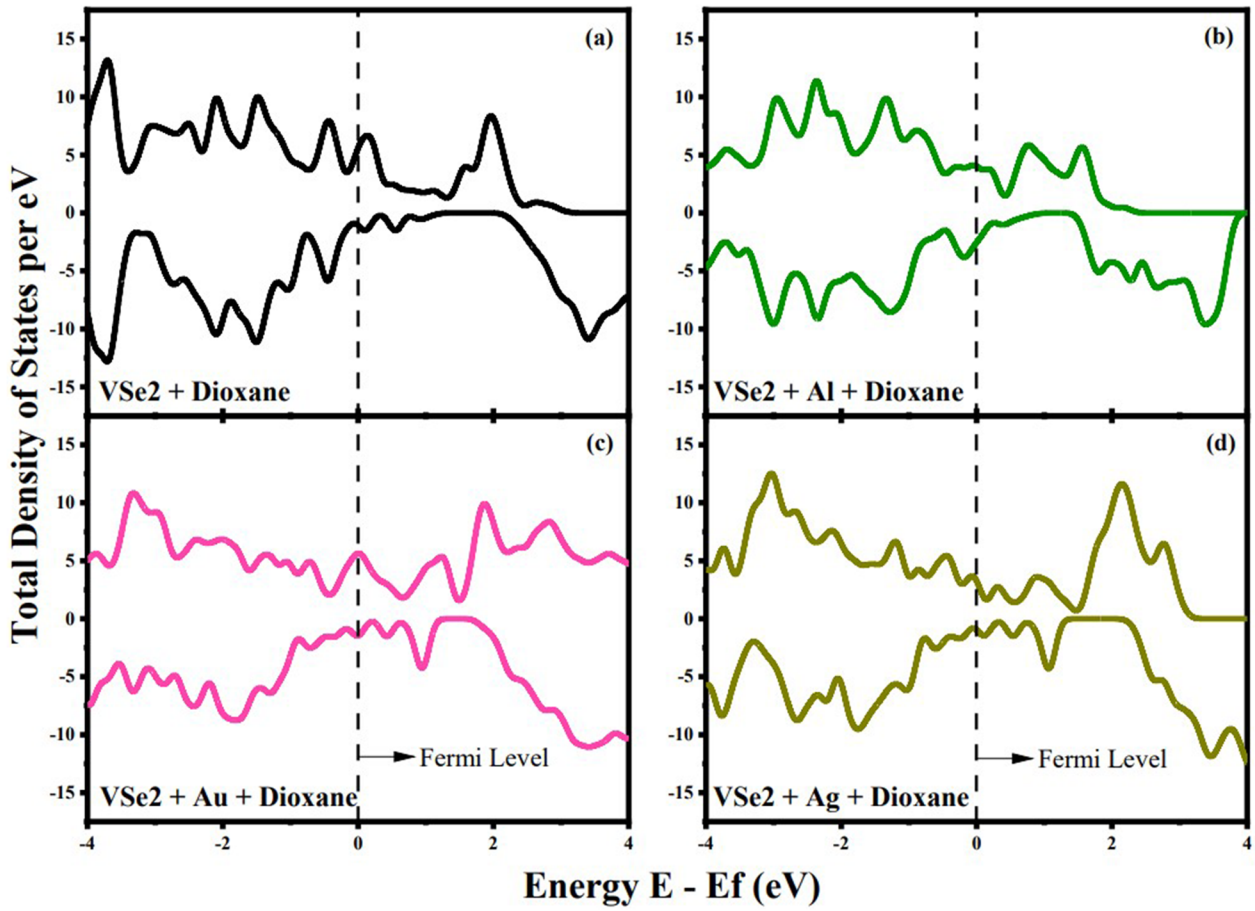

FIG. 8. TDOS plots of dioxane interaction on (a) pristine VSe_2, (b) VSe_2 + Al, (c) VSe_2 + Au, and (d) VSe_2 + Ag systems.

relaxed metal-doped VSe_2 system such that the distance between the metal and the molecule is ~2 Å. The resulting structural combinations are allowed to optimize geometrically. The corresponding structures in their minimum energy configurations are shown in Fig. 7.

The adsorption energy and bond length of dioxane on different VSe_2 systems are tabulated (Table II). The dioxane has a greater binding on the Al-doped system with an adsorption energy of −0.8 eV. This high energy value indicates that dioxane molecules chemisorb on the Al-doped system. While dioxane adsorption on the Ag- and Au-doped VSe_2 systems are mostly physisorption, the adsorption energies are −0.30 and −0.20 eV, respectively. It is also noted that the dioxane adsorption strength increases by the strategy of metal doping, which in turn signifies the improvement in the sensing activity of the pristine VSe_2 system. The shortest distance between the O atom of the dioxane molecule and the Al atom in the VSe_2 + Al system is 3.38 Å. While the O–Au and O–Ag distances are 2.26 and 2.62 Å, respectively. The adsorption energy calculations conclude that the Al-doped VSe_2 system is well suited as the sensor material for detecting dioxane molecules from the atmosphere.

E. Mechanism of dioxane adsorption in metal-doped VSe_2 system

The DOS analysis explains how the electronic structure of the metal-doped VSe_2 system varies with the dioxane adsorption. Figure 8 compares the TDOS of the pristine and metal-doped VSe_2 system after the dioxane adsorption. The main reason for the origin of new energy states of the pristine and metal-doped VSe_2 system near the Fermi level is mainly because of the presence of dioxane molecules on its surface.

We have also analyzed the PDOS to clarify the orbital level interactions and charge transfer in the metal-doped VSe_2 systems. The PDOS of the Al 3*p* orbitals of VSe_2 + Al and VSe_2 + Al + dioxane systems are shown in the left top and bottom panel, respectively, in Fig. 9. At the same time, the right upper panel of the same figure represents the PDOS for the O 2*p* orbitals of the isolated dioxane, and the lower panel compares the PDOS for the O 2*p* orbitals of the VSe_2 + Al + dioxane system. It is worth noting that, after the interaction of the dioxane molecule with the VSe_2 + Al system, the energy states around the Fermi level of the Al 3*p* orbital diminished. At the same time, new states originated around the Fermi level of

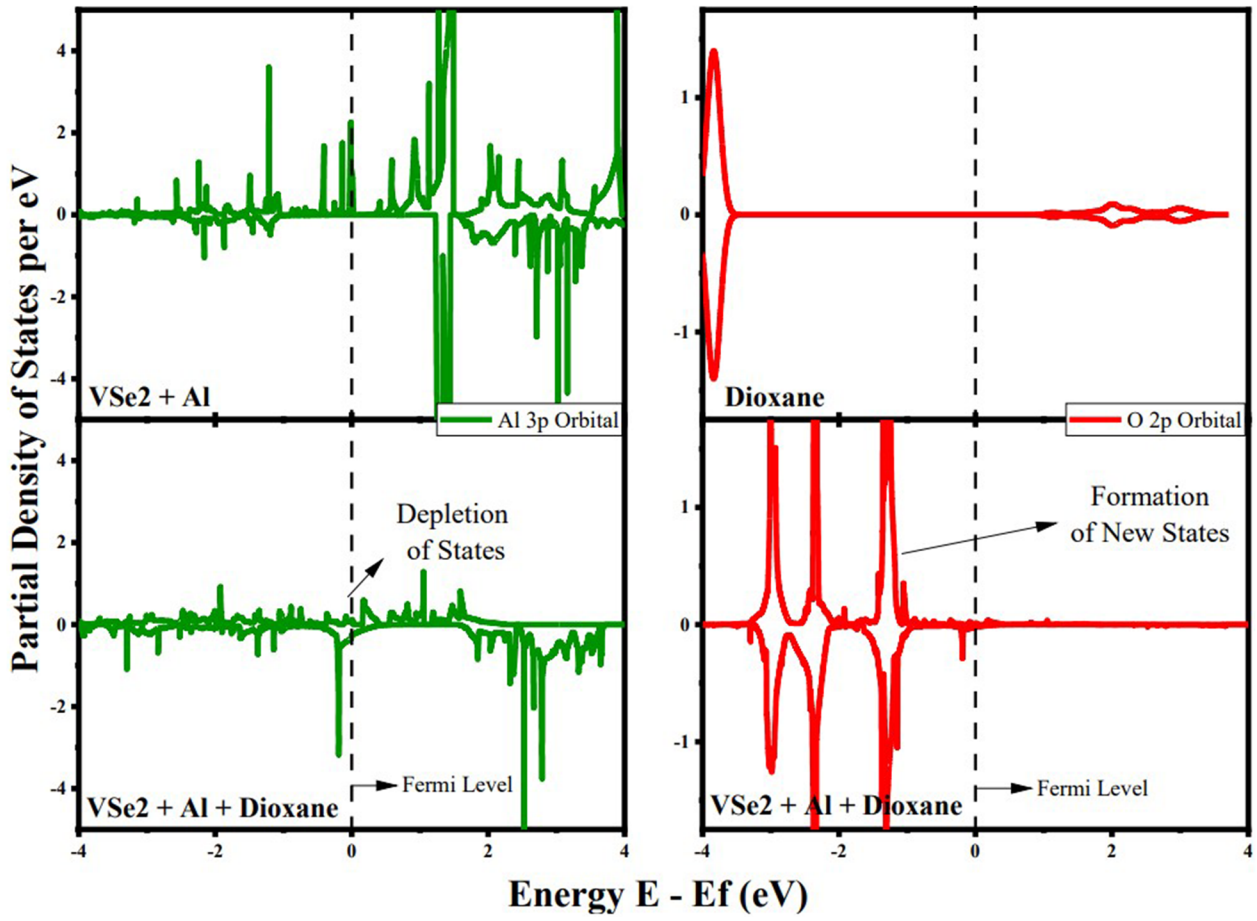

FIG. 9. Orbital interaction analysis of VSe_2 + Al + dioxane using PDOS plots, compare the valence orbitals of Al in the VSe_2 + Al and VSe_2 + Al + dioxane system in the left panel. In contrast, the right panel compares the 2*p* orbitals of isolated dioxane atoms and the VSe_2 + Al + dioxane systems.

TABLE III. LCA information on charge transfer of VSe_2 + metal systems to the dioxane molecule.

System	Charge transfer
VSe_2 + Al + dioxane	−0.567*e* (Al 3*p* orbital – O 2*p* orbital)
VSe_2 + Au + dioxane	−0.101*e* (Au 6*s* orbital – O 2*p* orbital)
VSe_2 + Ag + dioxane	−0.132*e* (Ag 5*s* orbital – O 2*p* orbital)

the O 2*p* orbital. These states were absent in the same energy range of the PDOS of isolated dioxane. This formation of new states in the O 2*p* orbital and decrement in the intensity of available energy states in the Al 3*p* orbital implies that the electronic charges are transferred from the O 2*p* to Al 3*p* orbital. In addition, the strong dioxane adsorption is because of the p-p orbital overlap. The quantitative charge transfer study by LCA also justifies this charge transfer, i.e., ~0.567*e* charges are lost by the 3*p* orbitals of Al in the VSe_2 + Al system to the O 2*p* orbital of the dioxane molecule.

A comparable reallocation of the energy states is observed in the PDOS of VSe_2 + Au and VSe_2 + Ag systems after the dioxane adsorption (Fig. S2). Similar to the Al 3*p* orbitals, the energy states of Ag 5*s* and Au 6*s* orbitals near the Fermi level decrease. Meanwhile, there is an enhancement in the energy states in the vicinity of the Fermi level of O 2*p* orbital of dioxane in the adsorbed system. The charge transfer from Ag and Au's *s* orbitals to the O 2*p* orbitals causes this reduction and enhancement in states. According to LCA, Au 6*s* lose 0.101*e*, and Ag 5*s* lose 0.132*e* charges to the O 2*p* orbital of dioxane, shown in Table III.

A large amount of charge transfer between the Al-doped VSe_2 system and dioxane molecule is due to the strong chemical adsorption. The minor charge transfer from the Ag and Au to the dioxane molecule is due to the physisorption. Since adsorption energy and charge transfer are the important parameters in sensing, the Al-doped VSe_2 system will be beneficial for the fabrication of electrochemical dioxane sensors.

IV. CONCLUSION

In conclusion, we used the first principle density functional theory technique to explore the dioxane sensing abilities of pristine and metal-doped (Al, Au, and Ag) 2D VSe_2 systems. We have investigated various adsorption sites of the dioxane molecules on the pristine VSe_2 surface. Our adsorption energy calculation suggests that the dioxane interaction is more with the metal-doped VSe_2 system, particularly the Al-doped VSe_2, than its pristine counterpart. The Al atom binds strongly on the VSe_2 surface than the other metals with higher energy and charge transfer. The metal doping improved the conductivity and hence the adsorption ability of the VSe_2 system. The strong adsorption of the dioxane molecules with the VSe_2 + Al system is mainly due to the extensive charge transport and orbital interaction between the O 2*p* of dioxane and the 3*p* orbitals of Al. The MD simulation at 300 K verified the room temperature stability of the VSe_2 + Al system; therefore, the Al-doped VSe_2 system could be a more promising dioxane sensor. This work aims to provide a theoretical foundation and an interpretation of the adsorption behaviors of VSe_2-based biosensors to facilitate future empirical creations.

SUPPLEMENTARY MATERIALS

See the supplementary material for the PDOS analysis of Au and Ag doping in pristine VSe_2 and the dioxane interaction on Au and Ag doped VSe_2.

ACKNOWLEDGMENTS

N.K. acknowledges SERB: CRG (Grant No. CRG/2021/001506), UGC: Special Assistance Program (SAP; Grant Nos. F.530/12/DRS/2009 and F.530/13/DRS II/2016), UGC: Scheme for Promotion of Academic and Research Collaboration (SPARC; Grant Nos. P930, P1400, P1429, and P1460), DST: Nano Mission [Grant No. SR/NM/NS-1420-2014(C)], DST: Fund for Improvement of S&T Infrastructure (FIST; Grant No. SR/FST/P SI-143/2009), DAE: UGC-Consortium for Scientific Research (CSR; Grant No. UGC-DAE-CSR-KC/CRS/19/RC08/0983/1018), DAE-Board of Research in Nuclear Sciences (BRNS; Grant No. 39/29/2015-BRNS/39009), and DST Promotion of University Research and Scientific Excellence [PURSE; Grant No. SR/S9/Z-23/2010/22(C, G)], Government of India programs for providing the facilities for research and development in IIUCNN, MGU. The authors would like to thank the High-Performance Computing facilities provided by MGU.

AUTHOR DECLARATIONS

Conflict of Interest

The authors have no conflicts to disclose.

Author Contributions

Sreejith Pallikkara Chandrasekharan: Conceptualization (equal); Data curation (equal); Formal analysis (equal); Funding acquisition (equal); Investigation (equal); Methodology (equal); Software (equal); Visualization (equal); Writing – original draft (equal); Writing – review & editing (equal). **Seetha Lakshmy**: Conceptualization (equal); Data curation (equal); Formal analysis (equal); Investigation (equal); Methodology (equal); Software (equal); Writing – original draft (equal); Writing – review & editing (equal). **Saju Joseph**: Conceptualization (equal); Data curation (equal); Formal analysis (equal); Investigation (equal); Methodology (equal); Project administration (equal); Software (equal); Supervision (equal); Writing – original draft (equal); Writing – review & editing (equal). **Nandakumar Kalarikkal**: Conceptualization (equal); Formal analysis (equal); Funding acquisition (equal); Project administration (equal); Resources (equal); Supervision (equal); Validation (equal); Writing – original draft (equal).

DATA AVAILABILITY

The data that support the findings of this study are available from the corresponding authors upon reasonable request.

REFERENCES

[1] A. Fullana, J. A. Conesa, R. Font, and S. Sidhu, "Formation and destruction of chlorinated pollutants during sewage sludge incineration," Environ. Sci. Technol. **38**(10), 2953–2958 (2004).

[2] H.-S. Iñaki, "Exploring the dissemination of environmental certifications in high and low polluting industries," J. Cleaner Prod. **89**, 50–58 (2015).

[3] R. Hu, S. Dai, D. Shao, A. Alsaedi, B. Ahmad, and X. Wang, "Efficient removal of phenol and aniline from aqueous solutions using graphene oxide/polypyrrole composites," J. Mol. Liq. **203**, 80–89 (2015).

[4] K. J. Godri Pollitt, J.-H. Kim, J. Peccia, M. Elimelech, Y. Zhang, G. Charkoftaki, B. Hodges, I. Zucker, H. Huang, N. C. Deziel, K. Murphy, M. Ishii, C. H. Johnson, A. Boissevain, E. O'Keefe, P. T. Anastas, D. Orlicky, D. C. Thompson, and V. Vasiliou, "1,4-dioxane as an emerging water contaminant: State of the science and evaluation of research needs," Sci. Total Environ. **690**, 853–866 (2019).

[5] D. K. Stepien, P. Diehl, J. Helm, A. Thoms, and W. Püttmann, "Fate of 1,4-dioxane in the aquatic environment: From sewage to drinking water," Water Res. **48**, 406–419 (2014).

[6] S. Zhang, P. B. Gedalanga, and S. Mahendra, "Advances in bioremediation of 1,4-dioxane-contaminated waters," J. Environ. Manage. **204**, 765–774 (2017).

[7] M. A. Beckett and I. Hua, "Elucidation of the 1,4-dioxane decomposition pathway at discrete ultrasonic frequencies," Envviron. Sci. Technol. **34**(18), 3944–3953 (2000).

[8] U. Karges, D. Ott, S. De Boer, and W. Püttmann, "1,4-dioxane contamination of German drinking water obtained by managed aquifer recharge systems: Distribution and main influencing factors," Sci. Total Environ. **711**, 134783 (2020).

[9] Y. Xiong, Q. Zhang, R. Wandell, S. Bresch, H. Wang, B. R. Locke, and Y. Tang, "Synergistic 1,4-dioxane removal by non-thermal plasma followed by biodegradation," Chem. Eng. J. **361**, 519–527 (2019).

[10] C.-S. Lee, A. K. Venkatesan, H. W. Walker, and C. J. Gobler, "Impact of groundwater quality and associated byproduct formation during UV/hydrogen peroxide treatment of 1,4-dioxane," Water Res. **173**, 115534 (2020).

[11] M. J. Zenker, R. C. Borden, and M. A. Barlaz, "Occurrence and treatment of 1,4-dioxane in aqueous environments," Environ. Eng. Sci. **20**(5), 423–432 (2003).

[12] M. M. Rahman, A. Wahid, and A. M. Asiri, "Development of highly sensitive 1,4-dioxane sensor with semiconductor NiO-doped Nd_2O_3 nanostructures by electrochemical approach," New J. Chem. **43**(44), 17395–17402 (2019).

[13] T. K. Sana Fathima, A. Arshiya Banu, T. Devasena, and S. Ramaprabhu, "A novel, highly sensitive electrochemical 1,4-dioxane sensor based on reduced graphene oxide–curcumin nanocomposite," RSC Adv. **12**(30), 19375–19383 (2022).

[14] R. G. Parr, "Density functional theory of atoms and molecules," in *Horizons of Quantum Chemistry* (Springer, 1980), pp. 5–15.

[15] Z. Chen, Y. Liu, S. Liao, N. Yi, and Q. Hu, "Treatment of adsorption of dioxane by using SiCNT toward efficient remediation of refractory organic contaminants from wastewater: DFT and DFTB-MD simulations," J. Mol. Liq. **316**, 113869 (2020).

[16] Q. H. Wang, K. Kalantar-Zadeh, A. Kis, J. N. Coleman, and M. S. Strano, "Electronics and optoelectronics of two-dimensional transition metal dichalcogenides," Nat. Nanotechnol. **7**(11), 699–712 (2012).

[17] B. Radisavljevic, A. Radenovic, J. Brivio, V. Giacometti, and A. Kis, "Single-layer MoS_2 transistors," Nat. Nanotechnol. **6**(3), 147–150 (2011).

[18] A. Vaidyanathan, S. Lakshmy, G. Sanyal, S. Joseph, N. Kalarikkal, and B. Chakraborty, "Nitrobenzene sensing in pristine and metal doped 2D dichalcogenide MoS_2: Insights from density functional theory investigations," Appl. Surf. Sci. **550**, 149395 (2021).

[19] S. Xu, Y. Zhang, F. Xu, C. Chen, and Z. Shen, "Theoretical study of the adsorption behaviors of gas molecules on the Au-functionalized MoS_2 nanosheets: A search for highly efficient gas sensors," Comput. Theor. Chem. **1188**, 112935 (2020).

[20] S. Lakshmy, G. Sanyal, A. Vaidyanathan, S. Joseph, N. Kalarikkal, and B. Chakraborty, "Catechol detection in pure and transition metal decorated 2D MoS_2: Acumens from density functional theory approaches," Appl. Surf. Sci. **562**, 150216 (2021).

[21] M. Chhowalla, D. Voiry, J. Yang, H. S. Shin, and K. P. Loh, "Phase-engineered transition-metal dichalcogenides for energy and electronics," MRS Bull. **40**(7), 585–591 (2015).

[22] M. Calandra, "Chemically exfoliated single-layer MoS_2: Stability, lattice dynamics, and catalytic adsorption from first principles," Phys. Rev. B **88**(24), 245428 (2013).

[23] M. Salavati and T. Rabczuk, "Application of highly stretchable and conductive two-dimensional 1T VS_2 and VSe_2 as anode materials for Li-, Na- and Ca-ion storage," Comput. Mater. Sci. **160**, 360–367 (2019).

[24] C. Ataca, H. Şahin, and S. Ciraci, "Stable, single-layer MX_2 transition-metal oxides and dichalcogenides in a honeycomb-like structure," J. Phys. Chem. C **116**(16), 8983–8999 (2012).

[25] Z. Zhang, J. Niu, P. Yang, Y. Gong, Q. Ji, J. Shi, Q. Fang, S. Jiang, H. Li, X. Zhou, L. Gu, X. Wu, and Y. Zhang, "Van der Waals epitaxial growth of 2D metallic vanadium diselenide single crystals and their extra-high electrical conductivity," Adv. Mater. **29**(37), 1702359 (2017).

[26] G. Sanyal, S. Lakshmy, A. Vaidyanathan, N. Kalarikkal, and B. Chakraborty, "Detection of nitrobenzene in pristine and metal decorated 2D dichalcogenide VSe_2: Perspectives from density functional theory," Surf. Interfaces **29**, 101816 (2022).

[27] G. V. Kamarchuk, A. V. Khotkevich, V. M. Bagatsky, V. G. Ivanov, P. Molinié, A. Leblanc, and E. Faulques, "Direct determination of Debye temperature and electron-phonon interaction in 1T VSe_2," Phys. Rev. B **63**(7), 073107 (2001).

[28] Z. Zhang, P. Yang, M. Hong, S. Jiang, G. Zhao, J. Shi, Q. Xie, and Y. Zhang, "Recent progress in the controlled synthesis of 2D metallic transition metal dichalcogenides," Nanotechnology **30**(18), 182002 (2019).

[29] K. Xu, P. Chen, X. Li, C. Wu, Y. Guo, J. Zhao, X. Wu, and Y. Xie, "Ultrathin nanosheets of vanadium diselenide: A metallic two-dimensional material with ferromagnetic charge-density-wave behavior," Angew. Chem., Int. Ed. **52**(40), 10477–10481 (2013).

[30] R. Atkins, M. Dolgos, A. Fiedler, C. Grosse, S. F. Fischer, S. P. Rudin, and D. C. Johnson, "Synthesis and systematic trends in structure and electrical properties of $[(SnSe)_{1.15}]_m(VSe_2)_1$, $m = 1, 2, 3$, and 4," Chem. Mater. **26**(9), 2862–2872 (2014).

[31] A. L. Hector, M. Jura, W. Levason, S. D. Reid, and G. Reid, "Vanadium selenoether and selenolate complexes, potential single-source precursors for CVD of VSe_2 thin films," New J. Chem. **33**(3), 641–645 (2009).

[32] P. Giannozzi, S. Baroni, N. Bonini, M. Calandra, R. Car, C. Cavazzoni, D. Ceresoli, G. L. Chiarotti, M. Cococcioni, I. Dabo, A. Dal Corso, S. de Gironcoli, S. Fabris, G. Fratesi, R. Gebauer, U. Gerstmann, C. Gougoussis, A. Kokalj, M. Lazzeri, L. Martin-Samos, N. Marzari, F. Mauri, R. Mazzarello, S. Paolini, A. Pasquarello, L. Paulatto, C. Sbraccia, S. Scandolo, G. Sclauzero, A. P. Seitsonen, A. Smogunov, P. Umari, and R. M. Wentzcovitch, "QUANTUM ESPRESSO: A modular and open-source software project for quantum simulations of materials," J. Phys.: Condens. Matter **21**(39), 395502 (2009).

[33] J. P. Perdew, K. Burke, and M. Ernzerhof, "Generalized gradient approximation made simple," Phys. Rev. Lett. **77**(18), 3865–3868 (1996).

[34] J. Henke, F. Flicker, J. Laverock, and J. van Wezel, "Charge order from structured coupling in VSe_2," SciPost Phys. **9**(4), 056 (2020).

[35] A. Huang, C.-H. Chen, C.-H. Chang, and H.-T. Jeng, "Topological phase and quantum anomalous Hall effect in ferromagnetic transition-metal dichalcogenides monolayer $1T - VSe_2$," Nanomaterials **11**(8), 1998 (2021).

[36] B. Stahl and T. Bredow, "Critical assessment of the DFT + U approach for the prediction of vanadium dioxide properties," J. Comput. Chem. **41**(3), 258–265 (2020).

[37] Y. Wang, J. Wan, W. Tian, Z. Hou, X. Gu, and Y. Wang, "Theoretical screening of VSe_2 as support for enhanced electrocatalytic performance of transition-metal single atoms," J. Colloid Interface Sci. **590**, 210–218 (2021).